Article

An Efficient Hybrid Energy Harvesting Protocol for Cooperative NOMA Systems: Error and Outage Performance

Faical Khennoufa [1], Abdellatif Khelil [1], Khaled Rabie [2,*], Hakan Kaya [3] and Xingwang Li [4]

[1] LGEERE Laboratory, Department of Electrical Engineering, Echahid Hamma Lakhdar University, El-Oued, Algeria; khennoufa-faical@univ-eloued.dz, abdellatif-khelil@univ-eloued.dz.
[2] Department of Engineering, Manchester Metropolitan University, Manchester M1 5GD, U.K.; k.rabie@mmu.ac.uk.
[3] Electrical and Electronics Engineering, Zonguldak Bulent Ecevit University, Zonguldak, Turkey, 67100; hakan.kaya@beun.edu.tr
[4] School of Physics and Electronic Information Engineering, Henan Polytechnic University, Jiaozuo, China; lixingwang@hpu.edu.cn.
* Correspondence author.

Abstract: Cooperative non-orthogonal multiple access (CNOMA) has been recently adapted with energy harvesting (EH) to increase energy efficiency and extend the lifetime of energy-constrained wireless networks. In EH, two protocols are usually used for CNOMA, namely, power splitting (PS) and time switching (TS). In order to improve the existing EH protocols, this paper investigates a hybrid EH protocol-assisted CNOMA, which is a combination of the two aforementioned main existing EH protocols. The end-to-end bit error rate (BER) and outage probability (OP) expressions of users in our scheme are derived over Nakagami-*m* fading channels. For the sake of comparison and to highlight the achievable gains, the performance of the hybrid EH (HEH) protocol is compared with the benchmark schemes (i.e., existing EH protocols and no-EH). Based on extensive simulations, it is shown that the analytical results match perfectly with simulations which demonstrates the correctness of the derivations. Numerical results clearly indicate the superiority of the proposed scheme over all the considered benchmarks. In addition, we discuss the optimum value of EH factors to minimize the error and outage in the proposed scheme and show that an optimum value can be obtained according to channel parameters.

Keywords: BER, outage probability, cooperative, EH, hybrid and NOMA.

1. Introduction

Non-orthogonal multiple access (NOMA) is widely renowned for increasing the number of users and improving spectral efficiency in next-generation wireless networks [1–3]. Besides, NOMA can be easily integrated with other physical layer schemes. Hence, the cooperative-NOMA (CNOMA) has recently been received a great deal of attention due to its ability to increase spectral efficiency, user fairness and expand network coverage [4]. On the other hand, to increase energy efficiency and recharge the battery-limited devices, energy harvesting (EH) in CNOMA has been adopted [5,6]. In the literature, there are two major EH protocols, namely, power splitting (PS) and time switching (TS). In the PS protocol, the EH and information detection are performed simultaneously with a PS factor, whereas in the TS protocol, the EH and information detection are implemented at different time slots [7].

In the past years, the performances of NOMA schemes have been evaluated in terms of outage probability (OP) and ergodic capacity (EC) to prove the superiority of NOMA over OMA [8–13]. Also, to increase the system capacity, a nearly comprehensive analysis of CNOMA issues in terms of EC, OP with full-duplex (FD)/half-duplex (HD) in the presence of imperfect channel state information (ICSI), imperfect successive interference cancellation (ISIC) and imperfection of the hardware impairment has been performed [14–22]. Multiple relays scheme (e.g., selection and multi-hop relays) is one of the promising directions for increasing the system performance and expanding coverage area. In [23–25],

 doi:10.20944/preprints202212.0539.v1

the EC and OP for multiple relays have been evaluated. Also, the bit error rate (BER) is another key performance indicator (KPI) that has been examined for CNOMA FD/HD with single/multiple relays under the imperfection of the ICSI and ISIC [17,25–32]. Through the earlier literature, NOMA has the ability to serve multiple users at the same time and achieve superiority over OMA schemes in terms of OP and EC, while the error performance of OMA is better because NOMA schemes suffer from inter-user interference (IUI) [33]. Therefore, increasing the number of users will increase errors and reduce the performance of all NOMA schemes.

On the other hand, alternative wireless information and power transfer strategies are significant for the sustainable growth of wireless communications, especially with enormous energy consumption growth with ever-increasing connected devices [5,7]. In order to show the performance gain of EH-CNOMA over CNOMA without EH, the EC and OP of simultaneous wireless information and power transfer (SWIPT) aided CNOMA (SWIPT-CNOMA) have been evaluated [34–37]. The EH (TS and PS) for FD/HD CNOMA has been evaluated in terms of the OP and compared with conventional OMA [38]. In [39,40], the OP of CNOMA with PS has been performed. The OP, EC and throughput for TS selection relay CNOMA with the effect of ICSI and ISIC have been analyzed in [41]. In [42], TS FD CNOMA has been analyzed in terms of OP and throughput. A CNOMA for PS and TS has been investigated in terms of OP and EC over Nakagami-m fading channels [43]. A decode and forward (DF) CNOMA-assisted EH in three different EH protocols, namely: PS, TS, and ideal protocols with ISIC and ICSI have been implemented and compared in terms of the OP over Rayleigh fading channel [44]. The sum rate and energy efficiency have been examined for FD CNOMA with EH [45]. In [46], a PS CNOMA Internet-of-Things (IoT) network has been analyzed in terms of the OP under practical variations (ISIC and different incentive transmission power levels for the IoT). To handle the co-channel interference, the problem of joint power allocation and sub-channel assignment for Device-to-device (D2D)-enabled IoT NOMA, the sum rate, fairness, access rate and computational complexity have been investigated [47]. In [48], the CNOMA-IoT user scheduling strategy is used to enhance the secrecy OP. The authors in [49] evaluate overlay networks NOMA in terms of secrecy throughput and secrecy OP. In [50], the EH CNOMA for relay selection with ISIC over the Nakagami-m fading channel of the secrecy OP.

Regardless superiority of EH over schemes without EH, it is possible to improve EH to reach the best performance. Previously, an optimized protocol called hybrid EH that combines PS and TS jointly in order to improve the energy efficiency of EH OMA has been proposed and evaluated in terms of throughput [51]. According to the findings in [51], the hybrid protocol outperforms both TS and PS protocols. The hybrid protocol has been adopted to the EH CNOMA scheme in [52–54] to improve the performance of EH CNOMA. It has been analyzed in terms of EC and OP for CNOMA over the Rayleigh fading channel. These works do not provide a complete study of the hybrid protocol with their evaluation due to the following reasons: 1) The optimal value of the hybrid protocol has not been indicated compared to other EH protocols (i.e., PS and TS). 2) Does the hybrid protocol always outperform the existing EH protocols in all EH values? 3) Also, all these works assumed one of the users works as an assistant user to help the far user, so with only this assumption, the investigation is not enough. The case without the direct links between the source and users is very important to evaluate the performance. 4) All of these works analyze performance with the assumption of the Rayleigh fading channel, so the evaluation needs more realistic assumptions for the channel, e.g., the Nakagami-m fading channel, which is considered a practical fading channel.

Through examining the previous works, although most of the existing EH-CNOMA papers discuss investigating OP and EC, the error performance (one of the most important KPIs) investigation is very limited. In [29,55,56], the error performance of CNOMA with EH (with PS protocol) amplify-and-forward (AF) relay has been performed. The authors of [57] evaluated the error performance of the mth best relay selection in EH (with PS protocol) AF multiple relay-assisted CNOMA. Then in [58], the authors investigate the error performance

Preprints (www.preprints.org) | NOT PEER-REVIEWED | Posted: 28 December 2022 doi:10.20944/preprints202212.0539.v1

of CNOMA with an EH relay (with TS protocol). As seen above discussion, the related EH-CNOMA papers deal with only one EH harvesting protocol. However, a comparison of the existing EH protocols is important to select the proper protocol to guarantee the best performance in CNOMA.

As mentioned above, EH CNOMA for PS or TS has been implemented in [29,34–38,38–41,45,46,55–58], and OP, EC and BER have been analyzed. The comparison of the EH CNOMA schemes (TS and PS) is important to select which EH protocol is superior and which is performed in terms of OP and EC in [43,44]. To improve the EH CNOMA scheme, the hybrid protocol has been analyzed over the Rayleigh fading channel in terms of OP and EC in [52–54]. The channel behavior over large distances is not accurately predicted by the Rayleigh distribution. For more flexibility, Nakagami-m distribution represents a bigger range of channel models, which is considered a practical fading channel. According to the authors' best knowledge, the hybrid protocol has not been evaluated over the Nakagami-m fading channel. Therefore, we analyze and compare the OP of the hybrid protocol with the exiting EH protocols (i.e., PS and TS) and without EH over the Nakagami-m fading channel. Also, to the best of the authors' knowledge, most of the existing papers investigate the EH-CNOMA schemes by using either TS or PS protocol and no work provides hybrid EH for CNOMA in terms of BER. In addition, the BER performance of the EH-CNOMA schemes has not been studied well by considering different EH protocols. Motivated by the aforementioned discussions, in this paper, we investigate a hybrid EH protocol for CNOMA (HEH-CNOMA) in terms of BER and OP over the Nakagami-m fading channel. The main contributions of the paper are given as follows.

- We present the HEH-CNOMA scheme where the relay applies a hybrid EH protocol to improve the performance of the existing EH schemes in CNOMA networks.
- We also present three benchmark schemes (i.e., PS, TS and no-EH) to evaluate the performance of the HEH-CNOMA. We derive the exact end-to-end (e2e) BER expressions for HEH-CNOMA and three benchmarks over Nakagami-m fading channels. The simulations validate the perfect match of the analysis. Based on the extensive simulations, we reveal that the BER of HEH-CNOMA outperforms all three benchmarks remarkably.
- Also, we derive the exact e2e OP expressions for HEH-CNOMA and three benchmarks over Nakagami-m fading channels. The results are identical to simulations, and it shows the superiority of the hybrid protocol on all three benchmarks significantly.
- We also discuss the optimum values for EH parameters and power allocation (PA) coefficient in HEH-CNOMA in terms of BER and OP, and we present that optimum values can be obtained to improve the performance of both users.

The rest of the paper is presented as follows. The considered HEH-CNOMA system model is introduced along with three benchmark schemes in Section 1. In Section 2, we derive closed-forms analytical expressions of BER and OP of all schemes. The numerical results are presented in Section 3 to validate the analysis and compare it with the benchmarks. Finally, Section 4 concludes the paper.

2. System Model

We consider a CNOMA network consisting of a source (S), a DF relay (R), and two users named user 1 (U_1) and user 2 (U_2) as presented in Fig. 1. We assume that the R assists the users to receive the signal since the direct link between source and users does not exist due to large path-loss or obstacles. Each node is equipped with a single antenna. We suppose that the R node works in HD mode. All communication links are exposed to a Nakagami-m fading. The R node harvests energy from the radio frequency (RF) signal transmitted by the source (i.e., using three EH protocols defined below). In the second

Preprints (www.preprints.org) | NOT PEER-REVIEWED | Posted: 28 December 2022 doi:10.20944/preprints202212.0539.v1

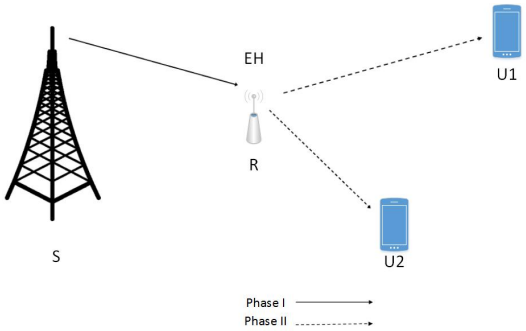

Figure 1. CNOMA assisted EH schemes.

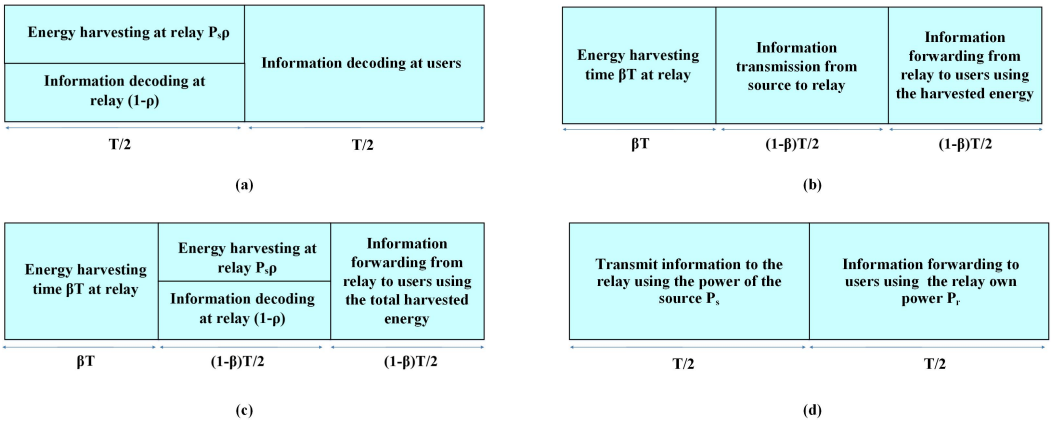

Figure 2. CNOMA assisted EH schemes: (a) PS protocol, (b) TS protocol, (c) Hybrid protocol and (d) No-EH.

phase, the R node forwards the signal to two users using the harvested energy [1]. The transmission block period is T. The EH protocols, namely i) PS; ii) TS; and iii) hybrid and their operations are described below.

- **PS**: In the first $T/2$ time slot, the received signal's power is split into two parts at the R: The first part (ρ) is used to harvest energy, while the second part (1-ρ) is utilized to decode data in the decoder (where ρ is the PS factor). The remaining time (i.e., $T2$) is devoted to delivering the data to the users (please see Fig. 2 (a)).
- **TS**: In the first βT time slot, the R harvests energy, where $0 \leq \beta \leq 1$ and β is the TS factor. Then, in the first $(1-\beta)T2$ of the remaining time, the S sends superimposed coding (SC) information to the R. Then, in the last $(1-\beta)T2$ time slot, the R uses the harvested energy to deliver this information signal to the users (please see Fig. 2 (b)).
- **Hybrid** : In the first βT time slot, the R harvests energy as being in TS mode, where $0 \leq \beta \leq 1$. Then, the S transmits an SC information to the R in the first $(1-\beta)T2$ of the remaining time. Also, during this first $(1-\beta)T2$ time period, the R harvest energy from the received information, where $0 \leq \rho \leq 1$ (ρ is the PS factor for energy harvesting during the first $(1-\beta)T2$ at the R). Subsequently, the R uses the harvested energy from βT plus $(1-\beta)T2$ time slots to forward the information signal to the users in the last $(1-\beta)T2$ (please see Fig. 2 (c)).
- **No-EH**: The R is not capable of harvesting energy, and it uses its own energy source (e.g., battery). The S and the R cover half of the communication ($T2$ time), and both consume equal power during these data transfers (as presented in Fig. 2 (d)).

[1] In this paper, in the EH schemes, we consider that the relay has no power to forward the signal in the second phase, so the relay can implement one of the EH schemes (PS, TS or hybrid) to forward the signal to users in the second phase using the harvested energy.

 doi:10.20944/preprints202212.0539.v1

At S, the messages of users are combined in an SC information signal with different power levels according to the users' channel gain[2] and the R receives this information signal in the first phase. Thus, the received information signal by the R node is given as

$$y_r = \sqrt{P_s \varpi}(\sqrt{\alpha_1} s_1 + \sqrt{\alpha_2} s_2) h_r + n, \tag{1}$$

where ϖ is the coefficient that indicates how much of the source power is dedicated to information transfer, it will be $(1-\rho)$ for PS and hybrid mode whereas equals to 1 for TS and no-EH modes. s_1 and s_2 are the U_1 and U_2 signals, respectively. α_1 and α_2 are the PA coefficients of U_1 and U_2, respectively in which $\alpha_1 > \alpha_2$, such that $\alpha_1 + \alpha_2 = 1$. P_s is the transmit power of the source. h_r is the Nakagami-m fading channel coefficient[3] between S-R. $n \sim \mathcal{CN}(0, \sigma^2)$ is the additive white Gaussian noise (AWGN). When the information signal is received, the R node decodes the s_1 firstly. Then, through the SIC, s_2 is recovered. Thus, the signal-to-interference plus noise ratio (SINR) of s_1 and s_2 at R are expressed, respectively, as

$$\gamma_{R,s_1} = \frac{P_s \varpi \alpha_1 |h_r|^2}{P_s \varpi \alpha_2 |h_r|^2 + \sigma^2}, \tag{2}$$

$$\gamma_{R,s_2} = \frac{P_s \varpi \alpha_2 |h_r|^2}{\sigma^2}. \tag{3}$$

For fairness, we consider the total consumed energy in all protocols is equal to ϵ_T. Thus, ϵ_T is consumed equally by the S and R in the no-EH mode, while it is consumed only by the S in EH protocols, the source power is expressed as

$$P_s = \phi P_T, \text{ where } P_T = \epsilon_T / T, \tag{4}$$

where ϕ is equal to 1 for no-EH, 2 for PS and $\frac{2}{\beta+1}$ for TS and hybrid. In EH protocols, the harvested energy during the power transfer in each protocol is given as

$$E_h = \begin{cases} \eta P_s \rho \frac{T}{2} |h_r|^2, & \text{PS}, \\ \eta P_s \beta T |h_r|^2, & \text{TS}, \\ \eta P_s (\frac{2\beta + \rho(1-\beta))}{2}) T |h_r|^2, & \text{Hybrid}, \end{cases} \tag{5}$$

where η $(0 \leq \eta \leq 1)$ is the energy conversion efficiency factor. Thus, the transmit power of the relay through the harvested energy is given by

$$P_r = \begin{cases} P_s |h_r|^2 \Psi, & \text{PS, TS and Hybrid}, \\ P_s, & \text{no-EH}, \end{cases} \tag{6}$$

where

$$\Psi = \begin{cases} \eta\rho, & \text{PS}, \\ 2\eta\beta(1-\beta), & \text{TS}, \\ \eta(\rho + 2\beta(1-\beta)), & \text{Hybrid}. \end{cases} \tag{7}$$

Based on the received information signal, the R implements maximum likelihood detection (MLD)/SIC, to detect s_1 and s_2 symbols, respectively. Based on the signals decoded in the previous phase, the R implements a new SC signal and by using the

[2] In the downlink NOMA system, the S or R combines the users' messages in an SC signal with different power levels according to the channel gains for each user, where the user with higher channel gain will mostly have less power. Thus, we take into account that the U_2 has a higher channel gain than U_1, i.e., $|h_1|^2 < |h_2|^2$.

[3] The envelope of h_r and h_k follows Nakagami-m fading with Ω_r and Ω_k spread and m_r and m_k shape parameters with m_r and m_k are greater than 1 [59].

Preprints (www.preprints.org) | NOT PEER-REVIEWED | Posted: 28 December 2022 doi:10.20944/preprints202212.0539.v1

harvested energy, it forwards this new SC signal to the users. The received information at the users is given by

$$y_k = \sqrt{P_r \varpi}(\sqrt{\alpha_1} s_1 + \sqrt{\alpha_2} s_2) h_k + n,\ k = 1, 2, \tag{8}$$

where h_k, $k = 1, 2$ is the Nakagami-m fading channel coefficient between $R-\mathrm{U}_k$. Through the information signal received by users, the U_1 detects its symbols s_1 directly, while the U_2 use the SIC to detect its symbols s_2. Hence, the SINRs at U_1 and U_2 are given as

$$\gamma_{U_1, s_1} = \frac{P_r \alpha_1 |h_1|^2}{P_r \alpha_2 |h_1|^2 + \sigma^2}, \tag{9}$$

$$\gamma_{U_2, s_1} = \frac{P_r \alpha_1 |h_2|^2}{P_r \alpha_2 |h_2|^2 + \sigma^2}, \tag{10}$$

$$\gamma_{U_2, s_2} = \frac{P_r \alpha_2 |h_2|^2}{\sigma^2}, \tag{11}$$

where P_r changes according to EH protocols as presented in (6).

3. Performance analysis

In this section, over the Nakagami-m fading channels, we derive the closed-form BER and OP of the two phases. Then, we obtain the e2e BER and OP expressions for each user.

3.1. BER

At both S and R, a binary phase-shift keying (BPSK) modulation is utilized to obtain the s_1 and s_2 signals. Hence, two different energy levels with similar probabilities could be presented. By using an MLD, for all EH protocols and no-EH, the R detects s_1 firstly by treating s_2 as noise. Thereafter, s_2 is detected using the SIC. Then, the R implements an SC signal again for the detected s_1 and s_2 symbols and forwards it to users by using the harvested energy (i.e., for the case of the EH protocols) or its own power (i.e., case of no-EH). Through MLD, U_1 detects its own symbols s_1, whereas U_2 uses a SIC to identify its symbols s_2. By using the common probability of independent error event in two phases, the e2e BER at each user is given as in [59] by

$$P_{e2e,k}(e) = 1 - \left(1 - P_{r,k}(e)\right)\left(1 - P_k(e)\right),\ k = 1, 2, \tag{12}$$

where $P_{r,k}(e)$ is the BER of U_k at the relay. $P_k(e)$ is the BER at U_k in the second phase.

3.1.1. BER in the first phase

Based on the discussion above (i.e., for EH and no-EH), R detects s_1 in the first step. The BER of s_1 at R, by following the steps in [25], can be given as

$$P_{r,1}(e) = \frac{1}{2} \sum_{i=1}^{2} \mathrm{Q}\left(\sqrt{\varpi \gamma \zeta_i |h_r|^2}\right), \tag{13}$$

where $\gamma = \frac{P_s}{\sigma^2}$, $\zeta_i = [(\sqrt{\alpha_1} + \sqrt{\alpha_2})^2, (\sqrt{\alpha_1} - \sqrt{\alpha_2})^2]$. The average BER (ABER) of (13) over a Nakagami-m fading channel by using [60] is given as

$$P_{r,1}(e) = \frac{1}{2} \sum_{i=1}^{2} \frac{1}{\sqrt{2\pi}} \frac{\Gamma(m_r + 0.5)}{\Gamma(m_r + 1)} \times \left(\frac{\sqrt{\varpi \gamma \zeta_i \delta / 2m_r}}{(1 + \sqrt{\varpi \gamma \zeta_i \delta / 2m_r})^{(m_r + 0.5)}}\right) \nabla_1(m_r, \varpi \gamma \zeta_i \delta), \tag{14}$$

where $\nabla_1(m_r, \varpi \gamma \zeta_i \delta) =_2 F_1(1, m_r + 0.5, m_r + 1, \frac{2m_r}{2m_r + \varpi \gamma \zeta_i \delta})$ and $\delta = \Omega_r$. ${}_2F_1(.,.;.,.)$ is the Gauss hypergeometric function.

We also need to analyze the BER performance of the correct and erroneous SIC as [25] to find the BER of s_2 at R. Thus, the BER performance of s_2 at R is given by

Preprints (www.preprints.org) | NOT PEER-REVIEWED | Posted: 28 December 2022 doi:10.20944/preprints202212.0539.v1

$$P_{r,2}(e) = \frac{1}{2}\sum_{j=1}^{5} \nu^j Q(\sqrt{\varpi\gamma\zeta_j|h_r|^2}), \tag{15}$$

where $\nu^j = [2, -1, 1, 1, -1]$, $\zeta_j = [\alpha_2, (\sqrt{\alpha_1}+\sqrt{\alpha_2})^2, (\sqrt{2\alpha_1}+\sqrt{\alpha_2})^2, (\sqrt{\alpha_1}-\sqrt{\alpha_2})^2, (2\sqrt{\alpha_1}-\sqrt{\alpha_2})^2]$. By using [60], the ABER of (15) over the Nakagami-m fading channel can be given as

$$P_{r,2}(e) = \frac{1}{2}\sum_{j=1}^{5} \nu^j \frac{1}{\sqrt{2\pi}}\frac{\Gamma(m_r+0.5)}{\Gamma(m_r+1)} \times \left(\frac{\sqrt{\varpi\gamma\zeta_j\delta/2m_r}}{(1+\sqrt{\varpi\gamma\zeta_j\delta/2m_r})^{(m_r+0.5)}}\right)\nabla_2(m_r, \varpi\gamma\zeta_j\delta), \tag{16}$$

where $\nabla_2(m_r, \varpi\gamma\zeta_j\delta) =_2 F_1(1, m_r+0.5, m_r+1, \frac{2m_r}{2m_r+\varpi\gamma\zeta_j\delta})$.

3.1.2. BER in the second phase

Using the harvested energy (i.e., using the power harvested of the three EH protocols as presented in section II), the R node forwards the SC signal to the users. The U_1 detect its symbols directly using MLD, so the BER at U_1 can be given by

$$P_1(e) = \frac{1}{2}\sum_{i=1}^{2} Q(\sqrt{\gamma\zeta_i\psi|h_1|^2|h_r|^2}). \tag{17}$$

As seen in (17), the conditional BER includes multiplying of two random variables which belong to first and second phase link qualities. Although, the conditional BER in (17) defines the BER of second phase, it includes $|h_r|^2$ since the transmit power of the relay (i.e., P_r) is a function of it (6). Thus, the ABER of (17) can not be simply obtained by averaging Gamma distribution (i.e., the absolute square of Nakagami-m). Firstly, the joint probability density function (PDF) of $|h_1|^2|h_r|^2$ should be derived. By following steps in [59] through the PDF of the product of two chi-square distributions, the PDF can be obtained. After simplification and using [61, Eq. (3.478.4)], we derive the ABER of (17) by using the Meijer-G function [61, Eq.(9.311)] by following the steps of [59,62], and the closed-form ABER at U_1 is given as

$$P_1(e) = \frac{1}{4\sqrt{\pi}}\sum_{i=1}^{2} \Delta_1 G_{4\,5}^{3\,3}\left(\begin{matrix}0, 1-u_2, 0.5-u_2, 1-u_2 \\ 0.5u_1, -0.5u_1, 1-u_2, u_2, 0\end{matrix}\middle|\frac{\Delta_3}{4}\right), \tag{18}$$

where $u_1 = m_r - m_1$, $u_2 = 0.5(m_r+m_1)$, $\Delta_1 = \Delta_2(\frac{m_1\Omega_r}{m_r\Omega_1})^{\frac{u_1}{2}}(\frac{1}{\gamma\zeta_i\psi})^{u_2}$, $\Delta_2 = \frac{(\frac{mr}{\Omega_r})^{mr}(\frac{m1}{\Omega_1})^{m1}}{\Gamma(m_r)\Gamma(m_1)}$, $\Delta_3 = 2\sqrt{\frac{m_1 m_r}{\Omega_1\Omega_r\gamma\zeta_i\psi}}$, m_r and m_k are the Nakagami fading parameters.

Proof: Please see Appendix A.

Also, we obtain the BER at U_2 through the correct and erroneous SIC. Thus, the BER at U_2 is given by

$$P_2(e) = \frac{1}{2}\sum_{j=1}^{5} \nu^j Q(\sqrt{\gamma\zeta_j\psi|h_2|^2|h_r|^2}). \tag{19}$$

As discussed above, the ABER of (19) needs further modification. Thus, we find the ABER of (19) by using the same method of (18) and it is given as

$$P_2(e) = \frac{1}{4\sqrt{\pi}}\sum_{j=1}^{5} \nu^j \Delta_4 G_{4\,5}^{3\,3}\left(\begin{matrix}0, 1-u_4, 0.5-u_4, 1-u_4 \\ 0.5u_3, -0.5u_3, 1-u_4, u_4, 0\end{matrix}\middle|\frac{\Delta_6}{4}\right), \tag{20}$$

where $u_3 = m_r - m_2$, $u_4 = 0.5(m_r+m_2)$, $\Delta_4 = \Delta_5(\frac{m_2\Omega_r}{m_r\Omega_2})^{\frac{u_1}{2}}(\frac{1}{\gamma\zeta_j\psi})^{u_4}$, $\Delta_5 = \frac{(\frac{mr}{\Omega_r})^{mr}(\frac{m2}{\Omega_2})^{m_2}}{\Gamma(m_r)\Gamma(m_2)}$ and $\Delta_6 = 2\sqrt{\frac{m_2 m_r}{\Omega_2\Omega_r\gamma\zeta_j\psi}}$.

Preprints (www.preprints.org) | NOT PEER-REVIEWED | Posted: 28 December 2022 doi:10.20944/preprints202212.0539.v1

For the no-EH case, we analyze the ABER of U_1 and U_2 in the second phase by using the same method in the first phase. Finally, we obtain the e2e ABER expression of U_1 as

$$P_{e2e,1}(e) = 1 - \left(1 - \frac{1}{2}\sum_{i=1}^{2}\frac{1}{\sqrt{2\pi}}\frac{\Gamma(m_r+0.5)}{\Gamma(m_r+1)} \times \frac{\sqrt{\varpi\gamma\zeta_i\delta/2m_r}}{(1+\sqrt{\varpi\gamma\zeta_i\delta/2m_r})^{(m_r+0.5)}}\nabla_1(m_r,\varpi\gamma\zeta_i\delta)\right) \times \left(1 - \frac{1}{4\sqrt{\pi}}\sum_{i=1}^{2}\Delta_1 G_{4\,5}^{3\,3}\left(\begin{matrix}0,1-u_2,0.5-u_2,1-u_2\\ 0.5u_1,-0.5u_1,1-u_2,u_2,0\end{matrix}\middle|\frac{\Delta_3}{4}\right)\right) \tag{21}$$

By substituting (14) and (18) into (12). Also, by substituting (16) and (20) into (12), we get the e2e ABER expression of U_2 as

$$P_{e2e,2}(e) = 1 - \left(1 - \frac{1}{2}\sum_{j=1}^{5}\nu^j\frac{1}{\sqrt{2\pi}}\frac{\Gamma(m_r+0.5)}{\Gamma(m_r+1)} \times \frac{\sqrt{\varpi\gamma\zeta_j\delta/2m_r}}{(1+\sqrt{\varpi\gamma\zeta_j\delta/2m_r})^{(m_r+0.5)}}\nabla_2(m_r,\varpi\gamma\zeta_j\delta)\right) \times \left(1 - \frac{1}{4\sqrt{\pi}}\sum_{j=1}^{5}\nu^j\Delta_4 G_{4\,5}^{3\,3}\left(\begin{matrix}0,1-u_4,0.5-u_4,1-u_4\\ 0.5u_3,-0.5u_3,1-u_4,u_4,0\end{matrix}\middle|\frac{\Delta_6}{4}\right)\right) \tag{22}$$

3.2. Outage probability

In the literature, the outage is defined when the receiver cannot successfully decode the received signal. The outage is expressed when the capacity is less than the transmission rate. In this subsection, the e2e OP of the EH protocols (PS, TS and hybrid) and no-EH are derived over the Nakagami-m fading channel.

The outage of the U_1 information occurs when s_1 is not successfully decoded at the first and second phases (i.e, at R and U_1, respectively). Based on this explanation, the e2e OP of U_1 can be expressed as

$$P_{e2e,U_1}(out) = 1 - P\big(\min(\gamma_{R,s_1},\gamma_{U_1,s_1}) \geq \theta_1\big). \tag{23}$$

The derivation of (23) for U_1 can be given as

$$P_{e2e,U_1}(out) = 1 - \left(1 - e^{-\frac{m_r}{\Omega_r}\zeta_1}\sum_{t=0}^{m_r-1}\frac{1}{t!}\left(\frac{m_r}{\Omega_r}\zeta_1\right)^t\right) \times \left(1 - \frac{G_{1\,3}^{2\,1}\left(\begin{matrix}1\\ m_r,m_1,0\end{matrix}\middle|\frac{\lambda_1}{\Omega_r\Omega_1}\right)}{\Gamma(m_r)\Gamma(m_1)}\right), \tag{24}$$

where $\zeta_1 = \frac{\theta_1\sigma^2}{(\alpha_1-\alpha_2\theta_1)P_s\varpi}$, $\lambda_1 = \frac{\theta_1\sigma^2}{(\alpha_1-\alpha_2\theta_1)P_s\Psi\rho}$ and $\theta_i = 2^{R_i/\Xi} - 1$. R_i is target rate of s_1 and s_2, Ξ is equal to $\frac{1-\beta}{2}$ for TS and hybrid and $\frac{1}{2}$ for PS and no-EH. In the case of the no-EH, we calculate the OP of the link $R - U_1$ by the same method in the link $S - R$.

Proof: Please see Appendix B.

Likewise, the OP of U_2 occurs if one of the two following cases occurs at the two phases (i.e., at R and U_2). The first event is that R/U_2 fails to detect signal s_1. The second event is that R/U_2 fails to detect the signal s_2 when s_1 is successfully detected. Based on the above events, the e2e OP of U_2 can be expressed as

$$P_{e2e,U_2}(out) = 1 - \big(1 - P_{R,s_2}(out)\big)\big(1 - P_{U_2,s_2}(out)\big), \tag{25}$$

where $P_{R,s_2}(x)$ and $P_{U_2,s_2}(x)$ are OP at R and U_2 in the first and second phases, respectively. As explained above, the OP of s_2 at R can be expressed as

$$P_{R,s_2}(out) = 1 - e^{-\frac{m_r}{\Omega_r}(\zeta_1+\zeta_2)}\sum_{t=0}^{m_r-1}\sum_{k=0}^{m_r-1}\frac{1}{t!}\frac{1}{k!}\left(\frac{m_r}{\Omega_r}\zeta_1\right)^t\left(\frac{m_r}{\Omega_r}\zeta_2\right)^k, \tag{26}$$

Preprints (www.preprints.org) | NOT PEER-REVIEWED | Posted: 28 December 2022 doi:10.20944/preprints202212.0539.v1

where $\zeta_2 = \frac{\theta_2 \sigma^2}{\alpha_2 P_s \varpi}$.

Also, the OP of s_2 at U_2 in the second phase can be expressed as

$$P_{U_2,s_2}(out) = \Xi, \tag{27}$$

where $\Xi = \frac{G_{1\,3}^{2\,1}\left(\begin{smallmatrix}1\\ m_r,m_2,0\end{smallmatrix}\middle|\frac{\lambda_1}{\Omega_r\Omega_2}\right)}{\Gamma(m_r)\Gamma(m_2)} + \frac{G_{1\,3}^{2\,1}\left(\begin{smallmatrix}1\\ m_r,m_2,0\end{smallmatrix}\middle|\frac{\lambda_2}{\Omega_r\Omega_2}\right)}{\Gamma(m_r)\Gamma(m_2)} - \frac{G_{1\,3}^{2\,1}\left(\begin{smallmatrix}1\\ m_r,m_2,0\end{smallmatrix}\middle|\frac{\lambda_1}{\Omega_r\Omega_2}\right)}{\Gamma(m_r)\Gamma(m_2)} \frac{G_{1\,3}^{2\,1}\left(\begin{smallmatrix}1\\ m_r,m_2,0\end{smallmatrix}\middle|\frac{\lambda_2}{\Omega_r\Omega_2}\right)}{\Gamma(m_r)\Gamma(m_2)}$
and $\lambda_2 = \frac{\theta_2 \sigma^2}{\alpha_2 \psi P_s}$ is defined.

We substitute (26) and (27) into (25) to find the e2e OP of U_2 for EH CNOMA as given

$$P_{e2e,U_2}(out) = 1 - \left(e^{-\frac{m_r}{\Omega_r}(\zeta_1+\zeta_2)} \sum_{t=0}^{m_r-1} \sum_{k=0}^{m_r-1} \frac{1}{t!}\frac{1}{k!}\left(\frac{m_r}{\Omega_r}\zeta_1\right)^t \left(\frac{m_r}{\Omega_r}\zeta_2\right)^k\right) \times (1-\Xi) \tag{28}$$

In the case of the no-EH, we calculate the OP of s_2 in the link $R - U_2$ by using the same method in the link $S - R$.

4. Numerical Results

In this section, we validate the theoretical analysis by Monte Carlo simulations. In all figures, the lines represent the simulation results, while the markers represent the analytical results. The channel parameters for all simulations are given in Table I and in all simulations, $\eta = 0.95$, R_1=0.1, R_2=0.2 and for a fair comparison, the total transmit SNR is defined as $P_T N_0$. In the simulations, we use normalized i.e., T=1 transmission time.

In Fig. 3, we present ABER performances of both users for all protocols, where $\alpha_1 = 0.9$, and $\beta = \rho = 0.1$. Firstly, it is worth noting that our analysis matches perfectly with simulations in all protocols and scenarios which proves the correctness of our closed-from expressions. In addition, the analysis refers to both integer and noninteger values of m and it can be seen that this shape parameter m drives the diversity order. In Fig. 3, we can observe that the HEH-CNOMA outperforms all three benchmarks. By examining the comparisons in Fig. 3, we observe that the performance in Scenario I is better than in Scenario III and in the same manner the performance in Scenario IV is superior to Scenario II. These observations are a natural expectation of channel quality differences in various scenarios. The shape parameter in Scenario I is greater than in Scenario III so that Scenario I has better ABER performance and improved diversity order since in both phases less erroneous detection is performed. Likewise, Scenario IV outperforms Scenario II since the spread parameters are higher, which improves the performance. On the other hand, please note that in Scenario I and Scenario IV, the linear sum of spread parameters (i.e., $\Omega_r + \Omega_k$) of links are fixed which can reflect the relay position. In other words, the higher Ω_r means that the relay is closer to the source than the users. By comparing the performances of Scenario I and Scenario IV, we can observe that Scenario IV is superior. Thus, we can easily say that the CNOMA schemes have better performance when the relay is close to the middle of the source and users.

Table 1. Channel parameters in simulations.

	Ω_r	Ω_1	Ω_2	m_r	m_1	m_2
Scenario I	10	2	10	1.5	1.5	1.5
Scenario II	2	2	10	1.5	1.5	1.5
Scenario III	10	2	10	1	1	1
Scenario IV	8	4	12	1.5	1.5	1.5

The PA has prevailing effects on the ABER performance. To this end, to discuss the optimal PA, in Fig. 4, we present the ABER performance of users in Scenario I for $P_T N_0 = 20$ dB. Regardless of the PA changes, the HEH-CNOMA still outperforms all three benchmarks. Nevertheless, as expected, with the increase of α_2, the performance of U_1 is always decayed (i.e., ABER is increasing) since α_1 so the allocated power to U_1 symbols is

Preprints (www.preprints.org) | NOT PEER-REVIEWED | Posted: 28 December 2022 doi:10.20944/preprints202212.0539.v1

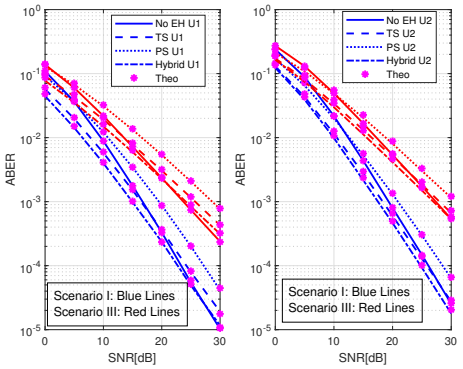

[Comparison between Scenarios I and III].

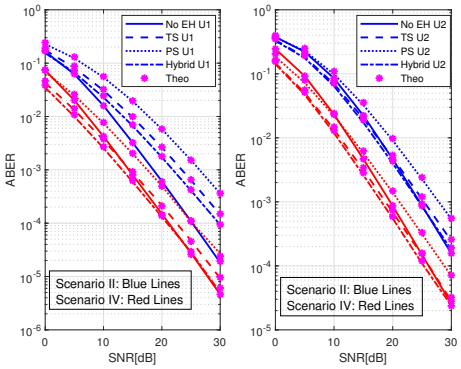

[Comparison between Scenarios II and IV]

Figure 3. ABER performance comparisons between HEH-CNOMA and benchmarks w.r.t. SNR.

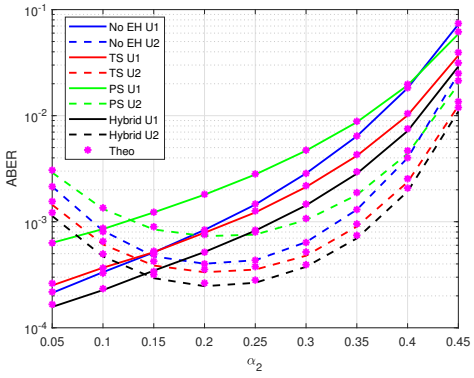

Figure 4. ABER performance comparisons between HEH-CNOMA and benchmarks w.r.t. PA.

Preprints (www.preprints.org) | NOT PEER-REVIEWED | Posted: 28 December 2022 doi:10.20944/preprints202212.0539.v1

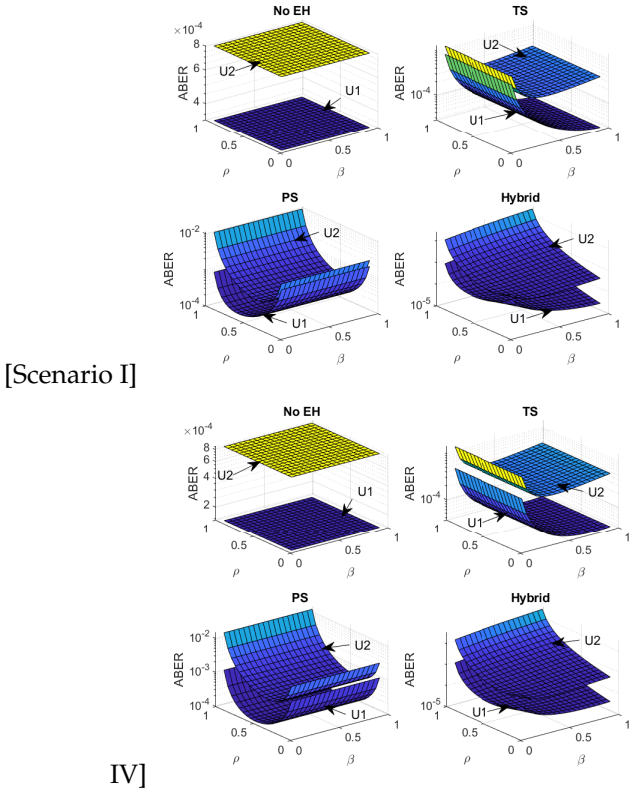

[Scenario I] [Scenario IV]

Figure 5. ABER performance comparisons between HEH-CNOMA and benchmarks w.r.t. EH parameters.

reduced. On the other hand, by increasing α_2, we firstly have better performance for 'U_2; however, it becomes worse with so much increase in α_2. This can be explained as follows. By increasing α_2, we allocate more power to U_2 symbols so that performance improves. However, U_2 should implement SIC (i.e., detect U_1 symbols firstly and subtract them) to detect its symbols. Therefore, if we increase α_2, U_1 symbols will be detected erroneously during SIC at the U_2 and it will cause an error floor in the detection of U_2 symbols. Based on the above discussion and Fig. 4, by considering both users' performances, we can say that the optimum value of PA should be $0.1 \leq \alpha_2 \leq 0.25$.

To better illustrate the effects of the EH parameters (β, ρ) on performance, in Fig. 5, we present ABER versus β and ρ in Scenario I and Scenario IV. In both comparisons, we can see that an optimal β-ρ pair can be obtained to minimize the ABER in HEH-CNOMA. According to channel conditions, β and ρ can be chosen jointly. For instance, in Scenario I, since the relay is close to the source, the link between S-R has already a good quality and less erroneous detection is performed at the relay. Therefore, we can increase β and ρ to increase the EH to guarantee reliable communication in the second phase by increasing the transmit power of the relay. On the other hand, when the relay is located near the middle (that is, Scenario IV), we should select lower values β and ρ. If we choose β and ρ too much, the information processing in the first phase becomes unreliable since less power is devoted to information transfer. In addition to this, the channel quality of the first phase is relatively worse, so the relay makes more errors in the detection, and this causes an error propagation from the relay to users.

Furthermore, we evaluate the OP performance for all protocols with four Scenarios as presented in Fig. 6. In this figure, we observe that the OP performance of the HEH-CNOMA is superior to all three benchmarks. By implementing the comparisons in Fig. 6, we observe that as in the ABER, the performance in Scenario I is better than in Scenario III. Likewise, Scenario IV has a better performance gain than Scenario II. Thus, we can see that the higher shape parameter value minimizes the OP performance and improves the diversity order

Preprints (www.preprints.org) | NOT PEER-REVIEWED | Posted: 28 December 2022 doi:10.20944/preprints202212.0539.v1

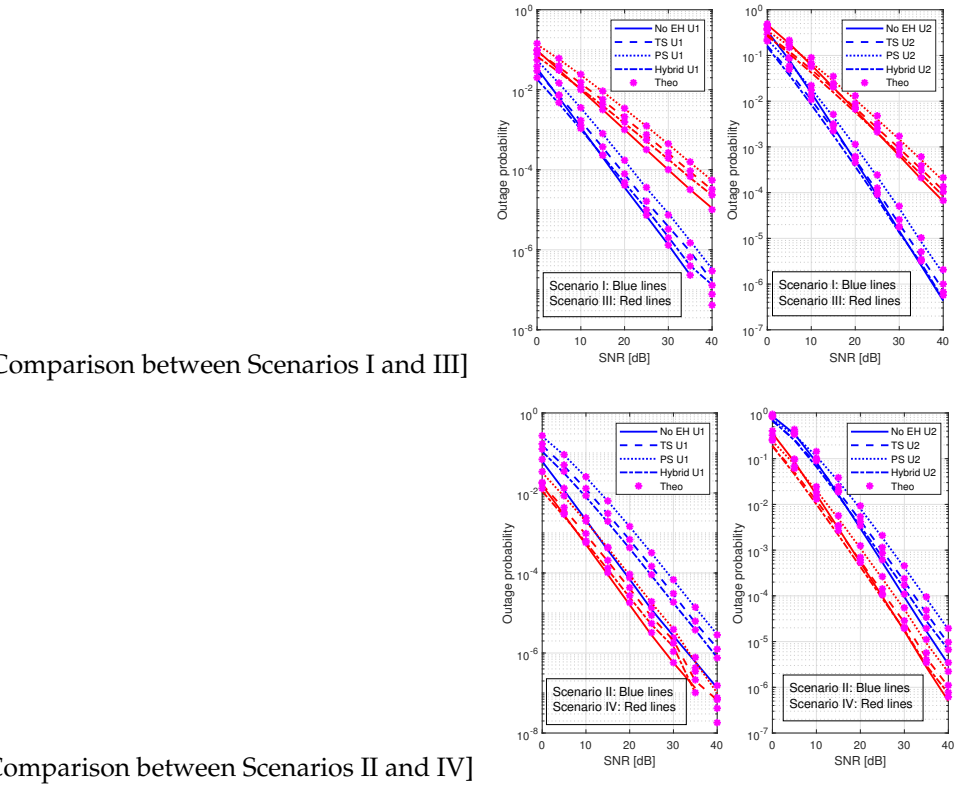

Figure 6. OP performance comparisons between HEH-CNOMA and benchmarks w.r.t. SNR.

since a lower OP is obtained in both phases. Also, as we can see, the lower values of spread parameters mean poor channel gain between S-R. This affects the harvested power and the signal detection at the relay (as given in Eq (6), the harvested power is affected by the channel quality of the S-R link. Also, the detected signal in the first phase depends on the quality of the S-R link, which has an impact on the signal forwarded to the users in the second phase.) and causes degradation in the EH protocols' performances. Besides, we can see that the minimum OP of both users can be obtained when the relay position is close to the middle.

In order to show the effect of the PA on the OP performance, Fig. 7 presents the OP performance of users in Scenario I for $P_T N_0 = 20$ dB, R_1=0.1 and R_2=1.3. We observe that HEH-CNOMA is still superior to TS and PS. Also, growth of α_2 increases the OP of U_1 while improving the OP of U_2. It becomes worse with so much increase in α_2, where it becomes difficult to detect the signals and this is due to the convergence of the PA of the

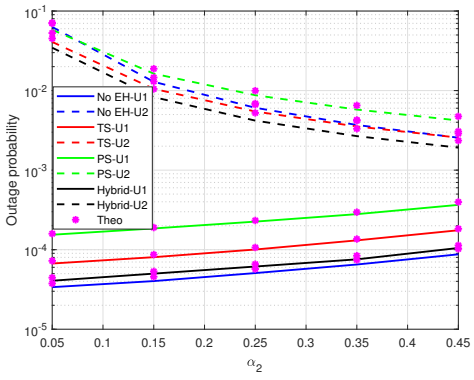

Figure 7. OP performance comparisons between HEH-CNOMA and benchmarks w.r.t. PA.

Preprints (www.preprints.org) | NOT PEER-REVIEWED | Posted: 28 December 2022 doi:10.20944/preprints202212.0539.v1

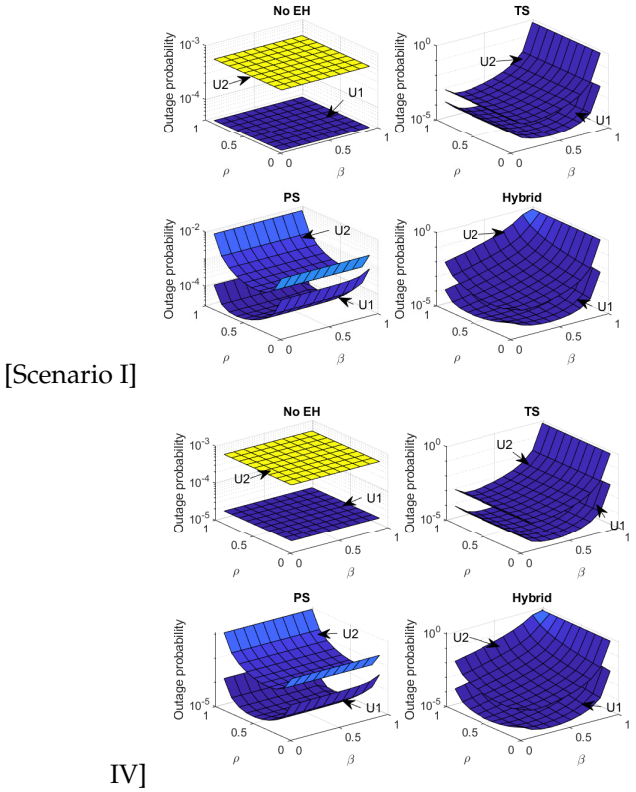

[Scenario I] [Scenario IV]

Figure 8. OP performance comparisons between HEH-CNOMA and benchmarks w.r.t. EH parameters.

users. Based on the above discussion and Fig. 7, considering both users' performances, the optimum PA value should be $0.1 \leq \alpha_2 \leq 0.25$.

To show the effects of the EH parameters (ρ, β) on the OP performance, Fig. 8 illustrates the performance of OP w.r.t. ρ and β in Scenario I and Scenario IV. In both comparisons, an optimal ρ-β pair can be indicated to reduce OP in the HEH-CNOMA. ρ and β can be selected jointly based on the channel conditions presented in the previous discussion, so the event is the same here for OP to reduce the outage. The near location of the relay means a good channel quality of the link S-R, and the event of an outage will be lower in this link. Hence, ρ and β can be increased to increase the harvested energy to achieve reliable communication in the second phase by increasing the relay transmit power. Likewise, as in Scenario IV, we need to choose lower values for ρ and β if the relay location is close to the middle. Because selecting higher values of ρ and β will increase the incidence of the outage in the first phase, this will affect information transmission in the second phase.

5. Conclusion

This paper investigates a hybrid protocol-assisted CNOMA, which is a combination of existing EH protocols (i.e., PS and TS). The aim of the study is to improve the performance of existing EH protocols with a more realistic protocol for practical assumptions. The e2e BER and OP expressions of users were analyzed over the Nakagami-m fading channel. The results illustrated that the HEH-CNOMA outperforms all benchmarks. More specifically, according to channel parameters, the performance gain of HEH-CNOMA over other schemes can be in the range of $1-3$dB and $0.5-1.5$dB for ABER and OP performances, respectively. This demonstrated that the same performance goals can be guaranteed with less power usage which is essential for energy-limited devices. Then, we discuss the optimal values of the hybrid protocol by considering PA and EH parameters. The optimal values of the EH factors and PA to achieve significantly better performance for both users jointly in HEH-CNOMA can be obtained according to the spread and shape parameters

 doi:10.20944/preprints202212.0539.v1

of the channel. We show that with the optimal parameter selection, the performance of HEH-CNOMA can be further improved and, in terms of ABER and OP, a 10 times better performance (e.g., $10^{-4} \rightarrow 10^{-5}$) can be achieved than any other EH scheme.

Author Contributions: Conceptualization, Khennoufa. F. and Khelil. A.; methodology, Khennoufa. F., Khelil. A., Rabie. K., Kaya. H and Li. X. ; software, Khennoufa. F. and Khelil. A.; validation, Khennoufa. F., Khelil. A., Rabie. K., Kaya. H and Li. X; formal analysis, Khennoufa. F. and Khelil. A.; investigation, Khennoufa. F., Khelil. A., Rabie. K., Kaya. H and Li. X; resources, Khennoufa. F. and Khelil. A; data curation, Khennoufa. F. and Khelil. A.; writing—original draft preparation, Khennoufa. F. and Khelil. A.; writing—review and editing, Khennoufa. F., Khelil. A., Rabie. K., Kaya. H and Li. X; visualization, Khennoufa. F. and Khelil. A.; supervision, Khelil. A.; project administration, Khennoufa. F. and Khelil. A..

Acknowledgments: The authors would like to thank Dr. Ferdi Kara (Department of Computer Engineering, Zonguldak Bulent Ecevit University, Zonguldak, Turkey) and Prof. Halim Yanikomeroglu (Department of Systems and Computer Engineering, Carleton University, Ottawa, Canada) for their great support and contribution to improving the quality of this paper.

Conflicts of Interest: The authors declare no conflict of interest

Appendix A

In the second phase, the R node uses the harvested power from the EH protocols as presented in section II to forward the SC signal to the users. The U_1 detects its symbols directly, so the BER at U_1 can be expressed by

$$P_1(e) = \frac{1}{2}\sum_{i=1}^{2} \mathrm{Q}\left(\sqrt{\gamma\zeta_i\psi|h_1|^2|h_r|^2}\right). \tag{A1}$$

Since (29) involves multiplying two random variables that are related to the qualities of the first and second phase links. The BER of the PDF of Y=$|h_1|^2|h_r|^2$ jointly should be analyzed through the PDF of the product of two chi-square distributions. Thus, the ABER of Y is given as

$$P_1(e) = \frac{1}{2}\sum_{i=1}^{2} \int_0^{\infty} \mathrm{Q}\left(\sqrt{\gamma\zeta_i\psi Y}\right) f_Y(Y)dY, \tag{A2}$$

where $f_Y(Y)$ is the PDF of Y, which can be acquired by the PDF of the product of two chi-square distributions and can be defined after simplification using [61, 3.478,4] as

$$f_Y(Y) = 2\left(\frac{m_1\Omega_r}{\Omega_1 m_r}\right)^{\frac{u_1}{2}} \Delta_1 Y^{u_2-1}\mathrm{K}_{u_1}\left(\sqrt{2\frac{m_1 m_r}{\Omega_r\Omega_1}Y}\right), \tag{A3}$$

where $\mathrm{K}_v(.)$ is the modified Bessel function of the second kind and is given in [61, Eq. (8.446)]. By applying $\mathrm{Q}(\sqrt{2x}) = 0.5\ \mathrm{erfc}(\sqrt{x})$ and using the Meijer-G function [61, Eq. (9.3)] conversions as in [**?** , Eq.(06.27.26.0006.01)] and [61, Eq.(9.34.3)] and we substitute these conversions into (30) with algebraic manipulations and by using [61, Eq. (9.311)] and [63, Eq. (14)], the closed-form ABER of U_1 in the second phase is obtained as

$$P_1(e) = \frac{1}{4\sqrt{\pi}}\sum_{i=1}^{2} \Delta_1 G_{4\,5}^{3\,3}\left(\begin{matrix}0,1-u_2,0.5-u_2,1-u_2\\ 0.5u_1,-0.5u_1,1-u_2,u_2,0\end{matrix}\middle|\frac{\Delta_3}{4}\right). \tag{A4}$$

By following the same method, we acquire the ABER of U_2 in the second phase.

Appendix B

The e2e OP of U_1 occurs when the SINRs of the two phases are less than the threshold θ_1. The e2e OP of U_1 is given by

$$P_{e2e,U_1}(out) = 1 - P\left(\min(\gamma_{R,s_1}, \gamma_{U_1,s_1}) \geq \theta_1\right). \tag{A5}$$

 doi:10.20944/preprints202212.0539.v1

Thus, (33) can be rewritten as

$$P_{e2e,U_1}(out) = 1 - P(\gamma_{R,s_1} \geq \theta_1)P(\gamma_{U_1,s_1} \geq \theta_1) \tag{A6}$$

By using the PDF and the cumulative distribution function (CDF) of the dedicated Nakagami-m channel as defined in [64, Eq. (19) and Eq. (20)], each term of (34) can be calculated, respectively, as

$$P(\gamma_{R,s_1} \geq \theta_1) = 1 - e^{-\frac{m_r}{\Omega_r}\zeta_1} \sum_{t=0}^{m_r-1} \frac{1}{t!}\left(\frac{m_r}{\Omega_r}\zeta_1\right)^t, \tag{A7}$$

$$P(\gamma_{U_1,s_1} \geq \theta_1) = P\Big(|h_r|^2|h_1|^2 \geq \lambda_1\Big). \tag{A8}$$

As we can see, (36) includes multiplying two random variables (RVs). Hence, the OP of the product of two RVs over the Nakagami-m fading for (36) is given as [65] by

$$\begin{aligned} P\Big(|h_r|^2|h_1|^2 \geq \lambda_1\Big) &= 1 - \int_0^\infty f_{|h_r|^2}(x)P\Big(|h_1|^2 \geq \lambda_1/x\Big)\,dx \\ &= 1 - \frac{1}{\Gamma(m_r)\Gamma(m_1)(\frac{\Omega_r}{m_r})^{m_r}} \times \\ &\int_0^\infty x^{m_r-1}e^{-\frac{m_r x}{\Omega_r}}\Gamma(m_1, \lambda_1 m_1/x\Omega_1)\,dx, \end{aligned} \tag{A9}$$

where $f_{|h_r|^2}(x)$ is the PDF of the dedicated Nakagami-m channel as defined in [64, Eq. (19)]. Thus, the integral of (37) is given in [66, Eq. (7)] by

$$P\Big(|h_r|^2|h_1|^2 \leq \lambda_1\Big) = 1 - \frac{G_{1\,3}^{2\,1}\left(\begin{matrix}1\\ m_r, m_1, 0\end{matrix}\middle|\frac{\lambda_1}{\Omega_r\Omega_1}\right)}{\Gamma(m_r)\Gamma(m_1)}. \tag{A10}$$

By substituting (35) and (38) into (34), we find the OP of U_1 for EH CNOMA as given in (24). We use the same steps to calculate the OP of U_2 for EH CNOMA.

References

1. Qi, Y.; Zhang, X.; Vaezi, M. Over-the-air implementation of NOMA: New experiments and future directions. *IEEE Access* **2021**, *9*, 135828–135844. https://doi.org/10.1109/ACCESS.2021.3116613.
2. Al-Abbasi, Z.Q.; Rabie, K.M.; So, D.K. EE optimization for downlink NOMA-based multi-tier CRANs. *IEEE Trans. Veh. Tech.* **2021**, *70*, 5880–5891.
3. Do, D.T.; Nguyen, T.T.T.; Le, C.B.; Voznak, M.; Kaleem, Z.; Rabie, K.M. UAV relaying enabled NOMA network with hybrid duplexing and multiple antennas. *IEEE Access* **2020**, *8*, 186993–187007.
4. Budhiraja, I.; Kumar, N.; Tyagi, S.; Tanwar, S.; Han, Z.; Piran, M.J.; Suh, D.Y. A systematic review on NOMA variants for 5G and beyond. *IEEE Access* **2021**, *9*, 85573–85644.
5. Ashraf, N.; Sheikh, S.A.; Khan, S.A.; Shayea, I.; Jalal, M. Simultaneous wireless information and power transfer with cooperative relaying for next-generation wireless networks: A review. *IEEE Access* **2021**, *9*, 71482–71504. https://doi.org/10.1109/ACCESS.2021.3078703.
6. Lin, S.; Tang, H.; Lu, B.; Shi, J. Energy Minimization for NOMA Cellular Networks with Two-Dimensional Resource Allocation. *IEEE Trans. Green Commun. Net.* **2022**.
7. Choi, H.H.; Lee, K. Cooperative Wireless Power Transfer for Lifetime Maximization in Wireless Multihop Networks. *IEEE Trans. Veh. Tech.* **2021**, *70*, 3984–3989.
8. Aghdam, M.R.G.; Tazehkand, B.M.; Abdolee, R. Joint Optimal Power Allocation and Beamforming for MIMO-NOMA in mmWave Communications. *IEEE Wirel. Commun. Lett.* **2022**, *11*, 938–941.
9. Sharma, P.; Kumar, A.; Bansal, M. Performance analysis of downlink NOMA over η–μ and κ–μ fading channels. *IET Commun* **2020**, *14*, 522–531.

10. Shi, Z.; Wang, H.; Fu, Y.; Yang, G.; Ma, S.; Ye, X. Outage performance and optimal design of MIMO-NOMA enhanced small cell networks with imperfect channel-state information. *China Commun.* **2021**, *18*, 107–128.
11. Ding, Z.; Yang, Z.; Fan, P.; Poor, H.V. On the performance of non-orthogonal multiple access in 5G systems with randomly deployed users. *IEEE Sign. Process. Lett.* **2014**, *21*, 1501–1505.
12. Sun, Y.; Ding, Z.; Dai, X. A new design of hybrid SIC for improving transmission robustness in uplink NOMA. *IEEE Trans. Veh. Tech.* **2021**, *70*, 5083–5087.
13. Li, X.; Zhao, M.; Zhang, C.; Khan, W.U.; Wu, J.; Rabie, K.M.; Kharel, R. Security analysis of multi-antenna NOMA networks under I/Q imbalance. *Elect.* **2019**, *8*, 1327.
14. Pei, X.; Yu, H.; Wen, M.; Mumtaz, S.; Al Otaibi, S.; Guizani, M. NOMA-based coordinated direct and relay transmission with a half-duplex/full-duplex relay. *IEEE Trans Commun* **2020**, *68*, 6750–6760.
15. Li, X.; Li, J.; Liu, Y.; Ding, Z.; Nallanathan, A. Residual transceiver hardware impairments on cooperative NOMA networks. *IEEE Trans. Wirel. Commun.* **2019**, *19*, 680–695.
16. Ma, L.; Li, E.; Yang, Q.; Wang, X.; Song, C. Performance Analysis and Optimization in Two-Way Cooperative NOMA Under Two-Phase Transmission Protocol. *IEEE Sys. J.* **2022**.
17. Kara, F.; Kaya, H. Improved user fairness in decode-forward relaying non-orthogonal multiple access schemes with imperfect SIC and CSI. *IEEE Access* **2020**, *8*, 97540–97556.
18. Kara, F.; Kaya, H. Threshold-based selective cooperative NOMA: Capacity/outage analysis and a joint power allocation-threshold selection optimization. *IEEE Commun. Lett.* **2020**, *24*, 1929–1933.
19. Liu, H.; Bai, Z.; Lei, H.; Pan, G.; Kim, K.J.; Tsiftsis, T.A. A new rate splitting strategy for uplink CR-NOMA systems. *IEEE Trans. Veh. Tech.* **2022**, *71*, 7947–7951.
20. Beddiaf, S.; Khelil, A.; Khennoufa, F.; Rabie, K. On the impact of IQI on cooperative NOMA with direct links in the presence of imperfect CSI. *Phy. Commun.* **2022**, p. 101952.
21. Do, D.T.; Nguyen, T.L.; Rabie, K.M.; Li, X.; Lee, B.M. Throughput analysis of multipair two-way replaying networks with NOMA and imperfect CSI. *IEEE Access* **2020**, *8*, 128942–128953.
22. Li, X.; Liu, M.; Deng, C.; Zhang, D.; Gao, X.C.; Rabie, K.M.; Kharel, R. Joint effects of residual hardware impairments and channel estimation errors on SWIPT assisted cooperative NOMA networks. *IEEE Access* **2019**, *7*, 135499–135513.
23. Yang, Z.; Ding, Z.; Wu, Y.; Fan, P. Novel relay selection strategies for cooperative NOMA. *IEEE Trans. Veh. Tech* **2017**, *66*, 10114–10123.
24. Xie, X.; Liu, J.; Huang, J.; Zhao, S. Ergodic capacity and outage performance analysis of uplink full-duplex cooperative NOMA system. *IEEE Access* **2020**, *8*, 164786–164794.
25. Khennoufa, F.; Abdellatif, K.; Kara, F. Bit error rate and outage probability analysis for multi-hop decode-and-forward relay-aided NOMA with imperfect SIC and imperfect CSI. *AEU-Internat. J. Electron. and Commun.* **2022**, *147*, 154124.
26. Kara, F.; Kaya, H. Error probability analysis of NOMA-based diamond relaying network. *IEEE Trans. Veh. Tech.* **2019**, *69*, 2280–2285.
27. Kara, F.; Kaya, H. Threshold-based selective cooperative-NOMA. *IEEE Commun. Lett.* **2019**, *23*, 1263–1266.
28. Shen, M.; Huang, Z.; Lei, X.; Fan, L. BER analysis of NOMA with max-min relay selection. *China Commun.* **2021**, *18*, 172–182.
29. Bariah, L.; Muhaidat, S.; Al-Dweik, A. Error probability analysis of NOMA-based relay networks with SWIPT. *IEEE Commun. Lett.* **2019**, *23*, 1223–1226.
30. Sashiganth, M.; Thiruvengadam, S.; Kumar, D.S. BER analysis of full duplex NOMA downlink and uplink co-operative user relaying systems over Nakagami-m fading environment. *Phy. Commun.* **2020**, *38*, 100963.
31. Hamza, A.A.; Dayoub, I.; Alouani, I.; Amrouche, A. On the error rate performance of full-duplex cooperative NOMA in wireless networks. *IEEE Trans. Commun.* **2021**, *70*, 1742–1758.
32. Safia, B.; Abdellatif, K.; Khennoufa, F.; Kara, F.; Kaya, H.; Li, X.; Rabie, K.; Yanikomeroglu, H. A unified performance analysis of cooperative NOMA with practical constraints: hardware impairment, imperfect SIC and CSI. *IEEE ACCESS* **2022**.
33. Kara, F.; Kaya, H. BER performances of downlink and uplink NOMA in the presence of SIC errors over fading channels. *IET Commun.* **2018**, *12*, 1834–1844.
34. Li, X.; Liu, M.; Deng, C.; Zhang, D.; Gao, X.C.; Rabie, K.M.; Kharel, R. Joint effects of residual hardware impairments and channel estimation errors on SWIPT assisted cooperative NOMA networks. *IEEE Access* **2019**, *7*, 135499–135513. https://doi.org/10.1109/ACCESS.2019.2942337.

35. Do, D.T.; Le, C.B. Impact of fixed power allocation in wireless energy harvesting NOMA networks. *Internat. J. Commun. Syst.* **2019**, *32*, 2–6. https://doi.org/10.1002/dac.4016.
36. Nayak, V.N.; Gurrala, K.K. A novel resource allocation for SWIPT-NOMA enabled AF relay based cooperative network. *Wirel. Pers. Commun.* **2021**, *118*, 2699–2716.
37. Jose, J.; Agarwal, A.; Krejcar, O.; Bhatia, V. Power controlled outage-aware optimal protocol for NOMA-assisted underlay D2D networks. *AEU-Internat. J. Elec. Commun.* **2022**, *157*, 154418.
38. Liu, C.; Zhang, L.; Chen, Z.; Li, S. Outage Probability Analysis in Downlink SWIPT-Assisted Cooperative NOMA Systems. *Journal of Communications and Information Networks* **2022**, *7*, 72–87.
39. Yu, Y.; Yang, Z.; Wu, Y.; Hussein, J.A.; Jia, W.K.; Dong, Z. Outage performance of NOMA in cooperative cognitive radio networks with SWIPT. *IEEE Access* **2019**, *7*, 117308–117317.
40. Ha, D.B.; Nguyen, S.Q. Outage performance of energy harvesting DF relaying NOMA networks. *Mob. Net. Appl.* **2018**, *23*, 1572–1585.
41. Bisen, S.; Shaik, P.; Bhatia, V. On performance of energy harvested cooperative NOMA under imperfect CSI and imperfect SIC. *IEEE Trans. Veh. Tech.* **2021**, *70*, 8993–9005, [2105.07047]. https://doi.org/10.1109/TVT.2021.3099067.
42. Aswathi, V.; Babu, A.V. Outage and throughput analysis of full-duplex cooperative NOMA system with energy harvesting. *IEEE Trans. Veh. Tech.* **2021**, *70*, 11648–11664.
43. Kader, M.F.; Uddin, M.B.; Islam, A.; Shin, S.Y. Cooperative non-orthogonal multiple access with SWIPT over Nakagami-m fading channels. *Trans. Emerg. Telecomm. Tech.* **2019**, *30*, e3571.
44. Kara, F. On the outage performance of SWIPT-NOMA-CRS with imperfect SIC and CSI. *Turk. J. Elec. Eng. Comp. Scien.* **2021**, *29*, 1139–1156.
45. Shirazi, M.; Zahabi, M. A Novel Full-duplex Relay Selection and Resource Management in Cooperative SWIPT NOMA Networks. *J. Elec. Comp. Eng. Innov. (JECEI)* **2022**.
46. Nguyen, M.T.; Vu, T.H.; Kim, S. Performance Analysis of Wireless Powered Cooperative NOMA-Based CDRT IoT Networks. *IEEE Sys. J.* **2022**.
47. Eslami, L.; Mirjalily, G. Fairness-aware resource allocation for D2D-enabled IoT in NOMA-based cellular networks with mutual successive interference cancellation. *Phy. Commun.* **2022**, p. 101901.
48. Largani, N.K.; Akhbari, B. Enhancing secrecy performance of energy harvesting NOMA systems using IoT user scheduling under untrusted users. *IET Commun.* **2022**.
49. Le-Thanh, T.; Ho-Van, K. Overlay networks with nonlinear energy scavenging and noma-assisted decoding: security performance analysis. *Arab. J. Scie. Eng.* **2022**, pp. 1–19.
50. Najimi, M. Energy harvesting relay selection and power allocation in cooperative secure NOMA networks with imperfect SIC over Nakagami-m channel. *J. Amb. Intell. Human. Comput.* **2022**, pp. 1–11.
51. Atapattu, S.; Evans, J. Optimal energy harvesting protocols for wireless relay networks. *IEEE Trans. Wirel. Commun.* **2016**, *15*, 5789 – 5803. https://doi.org/10.1109/TWC.2016.2569097.
52. Li, G.; Mishra, D.; Hu, Y.; Atapattu, S. Optimal designs for relay-assisted NOMA networks with hybrid SWIPT scheme. *IEEE Trans. Commun* **2020**, *68*, 3588–3601.
53. Amin, A.; Uddin, M.B.; Shin, S.Y. Performance enhancement of hybrid SWIPT protocol for cooperative NOMA downlink transmission. *arXiv preprint arXiv:1906.09159* **2019**.
54. Amin, A.A.; Shin, S.Y. Performance evaluation of cooperative NOMA-based improved hybrid SWIPT protocol. *arXiv preprint arXiv:2106.10799* **2021**.
55. Mohjazi, L.; Muhaidat, S.; Dianati, M. Performance analysis of differential modulation in SWIPT cooperative networks. *IEEE Sig. Proces. Lett.* **2016**, *23*, 620–624.
56. Li, S.; Bariah, L.; Muhaidat, S.; Sofotasios, P.; Liang, J.; Wang, A. Error analysis of NOMA-based user cooperation with SWIPT. In Proceedings of the 2019 15th Internat. Conf. Distr. Comput. Sens. Sys. (DCOSS). IEEE, 2019, pp. 507–513.
57. Li, S.; Bariah, L.; Muhaidat, S.; Sofotasios, P.C.; Liang, J.; Wang, A. SWIPT-enabled cooperative NOMA with mth best relay selection. *IEEE Open J. Commun. Soc.* **2020**, *1*, 1798–1807.
58. Khennoufa, F.; Abdellatif, K.; Kara, F. Bit error rate evaluation of relay-aided cooperative NOMA with energy harvesting under imperfect SIC and CSI. *Phy. Commun.* **2022**, *52*, 101630. https://doi.org/10.1016/j.phycom.2022.101630.
59. Babaei, M.; Aygölü, Ü.; Basar, E. BER analysis of dual-hop relaying with energy harvesting in Nakagami-*m* fading channel. *IEEE Trans. Wirel. Commun* **2018**, *17*, 4352–4361.
60. Simon, M.K.; Alouini, M.S. *Digital Communication over Fading Channels*; Wiley-IEEE Press, 2005; p. 936.
61. Gradshteyn, I.; Ryzhik, I. *Table of Integrals, Series, and Products*; Academic Press, 1994; [arXiv:1011.1669.]. https://doi.org/10.1016/b978-012294757-5/50002-7.

 doi:10.20944/preprints202212.0539.v1

62. Kara, F. Error performance of cooperative relaying systems empowered by SWIPT and NOMA. *Phy. Commun.* **2021**, *49*, 101450. https://doi.org/10.1016/j.phycom.2021.101450.
63. Adamchik, V.; Marichev, O. The algorithm for calculating integrals of hypergeometric type functions and its realization in REDUCE system. In Proceedings of the PISSAC, 1990, pp. 212–224.
64. Shukla, A.K.; Singh, V.; Upadhyay, P.K.; Kumar, A.; Moualeu, J.M. Performance analysis of energy harvesting-assisted overlay cognitive NOMA systems with incremental relaying. *IEEE Open J. Commun. Soc.* **2021**, *2*, 1558–1576.
65. Jain, N.; Bohara, V.A. Energy harvesting and spectrum sharing protocol for wireless sensor networks. *IEEE Wirel. Commun. Lett.* **2015**, *4*, 697–700.
66. Karagiannidis, G.K.; Tsiftsis, T.A.; Mallik, R.K. Bounds for multihop relayed communications in Nakagami-m fading. *IEEE Trans. Commun.* **2006**, *54*, 18–22.